

# A NOVEL APPROACH TO CONSTRAIN ROTATIONAL MIXING & CONVECTIVE-CORE OVERSHOOT IN STARS USING THE INITIAL-FINAL MASS RELATION

JEFFREY D. CUMMINGS<sup>1</sup>, JASON S. KALIRAI<sup>2,3</sup>, JIEUN CHOI<sup>4</sup>, C. GEORGY<sup>5</sup>,  
P.-E. TREMBLAY<sup>6</sup>, AND ENRICO RAMIREZ-RUIZ<sup>7</sup>

*Draft version January 11, 2019*

## ABSTRACT

The semi-empirical initial-final mass relation (IFMR) connects spectroscopically analyzed white dwarfs in star clusters to the initial masses of the stars that formed them. Most current stellar evolution models, however, predict that stars will evolve to white dwarfs  $\sim 0.1 M_{\odot}$  less massive than that found in the IFMR. We first look at how varying theoretical mass-loss rates, third dredge-up efficiencies, and convective-core overshoot may help explain the differences between models and observations. These parameters play an important role at the lowest masses ( $M_{\text{initial}} < 3 M_{\odot}$ ). At higher masses, only convective-core overshoot meaningfully affects white dwarf mass, but alone it likely cannot explain the observed white dwarf masses nor why the IFMR scatter is larger than observational errors predict. These higher masses, however, are also where rotational mixing in main sequence stars begins to create more massive cores, and hence more massive white dwarfs. This rotational mixing also extends a star's lifetime, making faster rotating progenitors appear like less massive stars in their semi-empirical age analysis. Applying the observed range of young B-dwarf rotations to the MIST or SYCLIST rotational models demonstrates a marked improvement in reproducing both the observed IFMR data and its scatter. The incorporation of both rotation and efficient convective-core overshoot significantly improves the match with observations. This work shows that the IFMR provides a valuable observational constraint on how rotation and convective-core overshoot affect the core evolution of a star.

## 1. INTRODUCTION

How mass loss, third dredge-up (hereafter 3DUP), convective-core overshoot (hereafter CCO), and rotation affect a star and its core evolution are long-standing challenges to model. Rotation is one of the most complex processes involved (e.g., Maeder & Meynet 2000, Langer 2012). Rapid rotation makes stars non-spherical, introducing strong changes to a star's observed characteristics, and rotation also introduces multiple types of interior mixing processes that non-, or slowly, rotating stars do not experience. This mixing can significantly affect how a star evolves by bringing fresh hydrogen into its core, prolonging the hydrogen burning phase and increasing the total mass of the hydrogen-exhausted core (e.g., Talon et al. 1997).

The MIST (Dotter 2016, Choi et al. 2016, 2017) and SYCLIST (Georgy et al. 2013, 2014) models consider the effects of rotation throughout all, if not nearly all, stages of stellar evolution. Both of these look at a broad range of

initial-rotation rates from non-rotating to  $\sim 0.80$  of critical rotation velocity and consider rotation's effect on a star's observed characteristics, their core evolution, and their lifetime. There exist several types of observations indicative of these effects: 1) Asteroseismology of rapidly rotating Be stars finds that they have abnormally high-mass cores (Neiner et al. 2012). 2) Observations of young clusters suggest that faster-rotating stars evolving more slowly is likely an important component of broad cluster turnoffs (e.g., Brandt et al. 2015, Niederhofer et al. 2015, D'Antona et al. 2015). 3) Rotational mixing in stars can help explain surface-abundance trends of various elements like carbon, nitrogen, and the light elements (e.g., Hunter et al. 2009, Proffitt et al. 2016, Cummings et al. 2017).

The consequences of rotation, in general, remain qualitatively consistent between various rotational models, but large differences remain in their predicted magnitudes. This is due to the complexity of rotation and rotational mixing, the difficulty of acquiring several of these observational tracers, that certain observations only trace mixing in the envelope, and that additional processes may affect these tracers.

Additional observational constraints on rotation would be valuable, and ideally ones that are sensitive to mixing at the cores of stars rather than only their outer envelopes. This letter analyzes how white dwarfs, the hot and exposed remnants of these stellar cores, can observationally constrain rotational mixing's and CCO's effect on core evolution.

This letter's structure is as follows: In Section 2 we discuss the initial-final mass relation of stars and the disagreements between observations and the available non-

<sup>1</sup> Center for Astrophysical Sciences, Johns Hopkins University, 3400 N. Charles Street, Baltimore, MD 21218, USA; jcummi19@jhu.edu

<sup>2</sup> Johns Hopkins University Applied Physics Laboratory, 11101 Johns Hopkins Road, Laurel, MD 20723, USA; Jason.Kalirai@jhuapl.edu

<sup>3</sup> Space Telescope Science Institute, 3700 San Martin Drive, Baltimore, MD 21218, USA

<sup>4</sup> Harvard-Smithsonian Center for Astrophysics, Cambridge, MA 02138, USA; jieun.choi@cfa.harvard.edu

<sup>5</sup> Geneva Observatory, University of Geneva, Maillettes 51, 1290 Sauverny, Switzerland; cyril.georgy@unige.ch

<sup>6</sup> Department of Physics, University of Warwick, Coventry CV4 7AL, UK; P-E.Tremblay@warwick.ac.uk

<sup>7</sup> Department of Astronomy and Astrophysics, University of California, Santa Cruz, CA 95064; enrico@ucolick.org

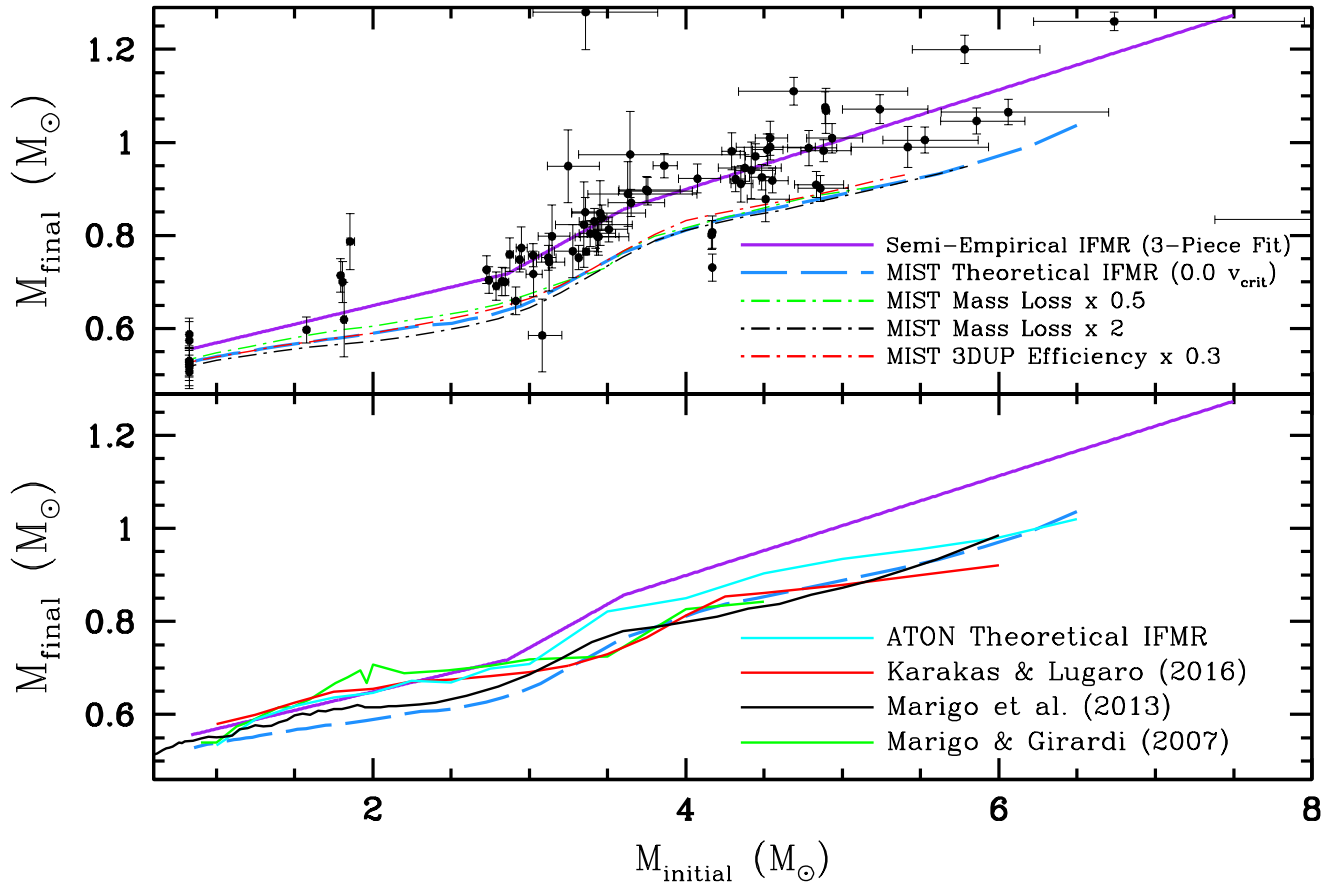


FIG. 1.— The upper panel compares the semi-empirical IFMR from Paper I to the non-rotating MIST theoretical IFMR. We illustrate that the IFMR has minor sensitivity to mass-loss rates and 3DUP efficiencies at the lowest masses ( $M_{\text{initial}} < 3 M_{\odot}$ ) and even less sensitivity at higher masses. The lower panel illustrates this further with independent theoretical IFMRs at solar metallicity, which show important differences at lower masses but are primarily consistent at higher masses. Only the ATON model with increased CCO predicts distinctly higher  $M_{\text{final}}$ , which can partially explain the offset from observations but not its intrinsic scatter.

rotating models. We also discuss stellar evolution’s sensitivity to mass-loss rates, 3DUP, and CCO. In Section 3 we demonstrate how the IFMR is sensitive to progenitor rotation rates and can constrain rotational mixing in the cores of stars. In Section 4 we summarize the results.

## 2. THE INITIAL-FINAL MASS RELATION

The initial-final mass relation (hereafter IFMR) compares a star’s initial main sequence mass to its final mass after it evolves to a white dwarf (hereafter WD) and has long been a tool to constrain stellar evolution models (e.g., Koester & Weidemann 1980). Semi-empirical IFMRs are commonly based on spectroscopic analysis of WDs in star clusters (e.g., Weidemann 2000, Kalirai et al. 2008, Cummings et al. 2016a, 2018; hereafter Paper I). Spectroscopic fitting of the Balmer lines in hydrogen-rich WDs measures both their  $T_{\text{eff}}$  and  $\log g$ . Applying these parameters to WD cooling models gives a WD’s current mass, luminosity, and cooling age, which is the time since it has left the tip of the asymptotic giant branch (hereafter AGB).

The method of deriving the IFMR first compares each WD’s spectroscopically derived photometry to its observed apparent photometry, which tests its cluster membership and single star status. The second step directly

compares a WD member’s cooling age to its cluster’s total age. This gives the evolutionary lifetime of its progenitor, and with application to models, ideally the same evolutionary models used to derive the cluster’s age, this yields the initial mass of each WD’s progenitor (Cummings & Kalirai 2018, Paper I).

The upper-panel of Figure 1 presents the semi-empirical IFMR from Paper I, which analyzed 80 WDs and used the MIST non-rotating models from Choi et al. (2016) to both derive cluster ages and infer  $M_{\text{initial}}$  (see Cummings & Kalirai 2018 for discussion of cluster age analysis). In solid purple, we show a linear 3-piece continuous fit, and in dashed-blue we show the theoretical non-rotating IFMR from MIST, which predicts progenitors will form WDs  $\sim 0.1 M_{\odot}$  less massive than observations. Additionally, even though this IFMR’s scatter has significantly decreased relative to previous semi-empirical IFMRs, the data’s  $M_{\text{initial}}$  and  $M_{\text{final}}$  errors have a moderate positive correlation (Cummings et al. 2016b), which makes the scatter at higher masses ( $> 3 M_{\odot}$ ) significantly larger than these observational and cluster-age errors can explain. Therefore, an intrinsic IFMR scatter may also be needed to explain observations.

In the upper-panel of Figure 1, we consider mass-loss rates in the MIST evolutionary models by increasing

(dashed-black) or decreasing (dashed-green) the applied mass-loss rate by a factor of 2 at *all* stages of evolution. This shows that while larger variations in mass-loss rates may play some role in lower-mass progenitors ( $< 3 M_{\odot}$ ), at higher masses (3 to  $6.5 M_{\odot}$ ) the WDs are increasingly insensitive to progenitor mass-loss rates.

This minor to very weak sensitivity to mass-loss rates at all phases is first because before the AGB, the standard mass-loss rates are negligible compared to the total mass of a star; hence, even large variations of mass-loss rates during these phases play little role in the core-evolution of a star. Second, during the AGB the mass-loss rates increase significantly, and in lower-mass stars, the core-masses grow as much as 30% in the thermally-pulsing AGB phase (e.g., Kalirai et al. 2014). Therefore, at these lower masses, an increase in the AGB mass-loss rate can cut this rapid core-mass growth short. At higher-masses, though, the thermally-pulsing AGB phase is rapid and little change in core mass occurs during this phase (e.g., Marigo et al. 2013). Moderately changing mass-loss rates or even introducing stochastic fluctuations in mass loss will not significantly affect the resulting WDs at higher masses (Doherty et al. 2014).

In the upper-panel of Figure 1, we also consider 3DUP efficiency, which plays a direct role in regulating the core-mass evolution during the thermally-pulsing AGB phase (Kalirai et al. 2014). More efficient 3DUP limits the core-mass growth during this phase while a lower efficiency lets the core grow with weaker reduction episodes. The dashed red line represents the theoretical MIST IFMR with 3DUP efficiency decreased to 30% of the standard. This shows it can affect WD masses, but even where it is the most important ( $\sim 4 M_{\odot}$ ) the resulting WDs are only increased in mass by  $\sim 0.02 M_{\odot}$ .

We additionally note that even though we are changing model parameters, these primarily only affect the relatively short AGB phase and have a negligible effect on theoretical evolutionary timescales. Hence, the semi-empirical  $M_{\text{initial}}$  are not affected.

These comparisons show that the uncertainties remaining in mass-loss rates and 3DUP may play a role in better matching WD masses, but at higher masses ( $> 3 M_{\odot}$ ) these uncertainties alone cannot explain observations. In the lower-panel of Figure 1 this is further illustrated by comparing multiple independent theoretical IFMRs. These IFMRs have important differences at lower masses, but virtually all models converge below observations at higher masses. The only theoretical IFMR with a meaningful difference is the ATON IFMR of Ventura et al. (2018), which adopts very similar physics to Karakas & Lugaro (2016) but with more CCO that leads to increased WD masses. The ATON model CCO also adopts the exponentially diffusive overshoot prescription, as do the MIST models, but again using a higher efficiency. This can partially explain the offset from observations but not its intrinsic scatter. Therefore, a non-standard process may be needed.

### 3. THE EFFECTS OF ROTATION ON THE IFMR

Stellar rotation induces mixing that drives additional hydrogen fuel into the core of a star, which has two consequences for the IFMR. First, faster-rotating progenitors evolve more massive cores, producing more massive WDs (Dominguez et al. 1996). In Figure 2 we show for

the MIST models the quantitative effects of rotation on the IFMR for stars at  $M_{\text{initial}}$  of 4, 5, and  $6 M_{\odot}$ . Each color represents a different initial rotation, with open circles representing the direct effect of how rotation creates higher-mass cores, leading to higher-mass WDs. This is a true shift of the IFMR to higher masses, creating an intrinsic spread in the IFMR due to the broad range of rotation rates observed in B dwarfs (e.g., Huang et al. 2010).

Second, faster rotating progenitors evolve more slowly. Therefore, in the IFMR analysis, a fast rotating progenitor will appear identical to a lower-mass slowly-rotating progenitor. This does not directly affect the true IFMR, but because non-rotating models have been adopted to infer  $M_{\text{initial}}$ , it introduces an offset in the determination of a WD's  $M_{\text{initial}}$ . In Figure 2 for each  $M_{\text{initial}}$  of 4, 5, and  $6 M_{\odot}$  we show with x's how much a given initial-rotation rate will cause the inferred  $M_{\text{initial}}$  to be underestimated. The solid circles in Figure 2 represent this effect in combination with the intrinsically higher-mass WDs. In the semi-empirical derivation of the IFMR, both of these factors combine to introduce a large scatter by shifting WDs formed by faster rotating progenitors to systematically higher masses and lower inferred  $M_{\text{initial}}$ .

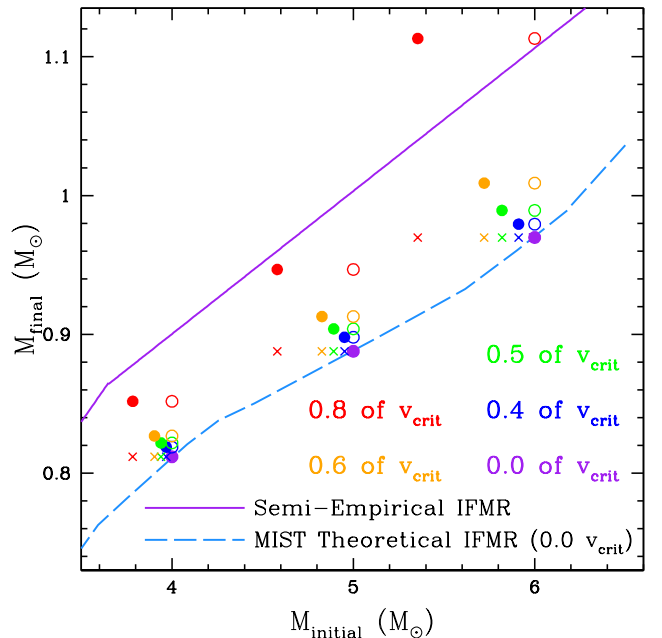


FIG. 2.— The effects of rotation in the MIST models at  $M_{\text{initial}}$  of 4, 5, and  $6 M_{\odot}$  for WD masses only (open circle), for systematic effects on the inference of  $M_{\text{initial}}$  from evolutionary timescales (x), and for these effects combined (solid circle). This can help to reproduce both the observed WD's higher masses and their scatter.

#### 3.1. Synthetic Initial-Final Mass Relation

While methods exist to measure WD rotations (e.g., Koester et al. 1998, Kilic et al. 2015), these observations are challenging. Further, it is difficult to use WD rotations to infer information about their progenitor's rotational histories (Kawaler 2015, Hermes et al. 2017). Therefore, with this large IFMR sample, we instead consider the effects of rotation statistically. Huang et al. (2010) observed young (high  $\log g$ ) B dwarfs (ranging

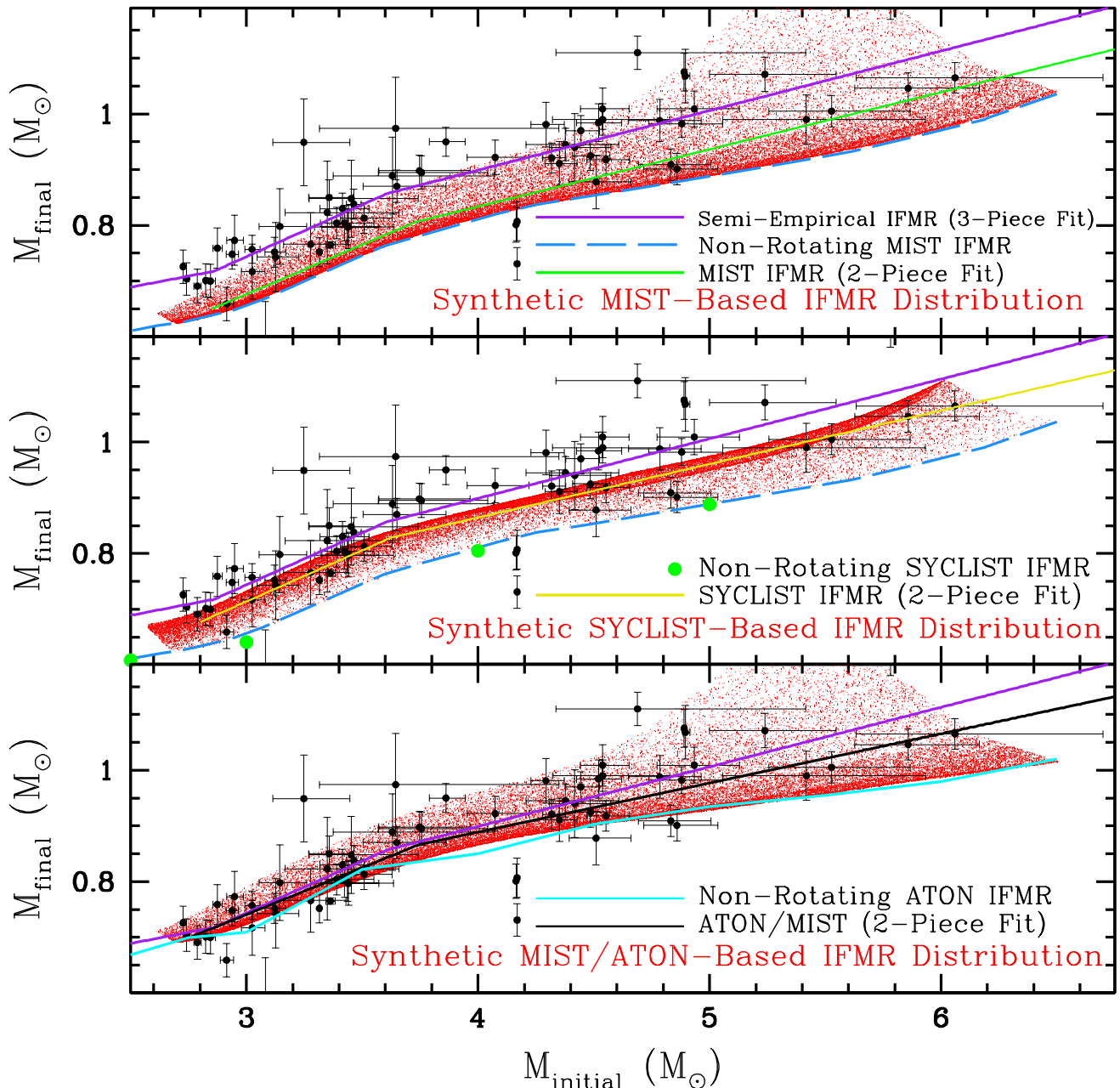


FIG. 3.— Application of the Huang et al. (2010) rotational distribution to the MIST rotational models (upper panel), to the SYCLIST rotational models (middle panel), and to the MIST rotational models applied to a smoothed ATON IFMR (lower panel). 2-piece fits are shown for the MIST distribution (green), the SYCLIST distribution (gold), and the MIST/ATON distribution (black). In the middle panel the consistency of the non-rotating SYCLIST IFMR (green data) and the non-rotating MIST IFMR (dashed blue) are shown.

from approximately 2 to 10  $M_{\odot}$ ) in the field and open clusters. They found a broad distribution of rotations spanning from several percent of  $v_{crit}$  to  $\sim 0.95$  of  $v_{crit}$ , with the most common rotation for young B dwarfs being  $\sim 0.49$  of  $v_{crit}$ . We note that their rotational distribution appears to be moderately sensitive to mass, with the higher masses still having a broad range of rotations but preferentially rotating at a lower percentage of their  $v_{crit}$ . The models of Rosen et al. (2012), however, find this results from more rapid angular momentum loss at higher masses and is not a result of slower initial rotation. Therefore, we will uniformly apply the total B-dwarf rotational distribution from Huang et al. (2010)

for all masses.

In the upper panel of Figure 3, we draw 40,000 synthetic stars in red (based on MIST rotational models) that are uniformly distributed in  $M_{initial}$  and follow the Huang et al. (2010) rotation distribution. This synthetic IFMR includes both the intrinsic increase in WD masses and, for the purpose of comparison to observations, the corresponding systematic estimate of a lower  $M_{initial}$ . This resulting scatter comes from the broad distribution of progenitor rotations, but note that the distribution remains concentrated at the lower envelope. This is because the MIST rotational models adopt a lower rotational-mixing efficiency and require above aver-

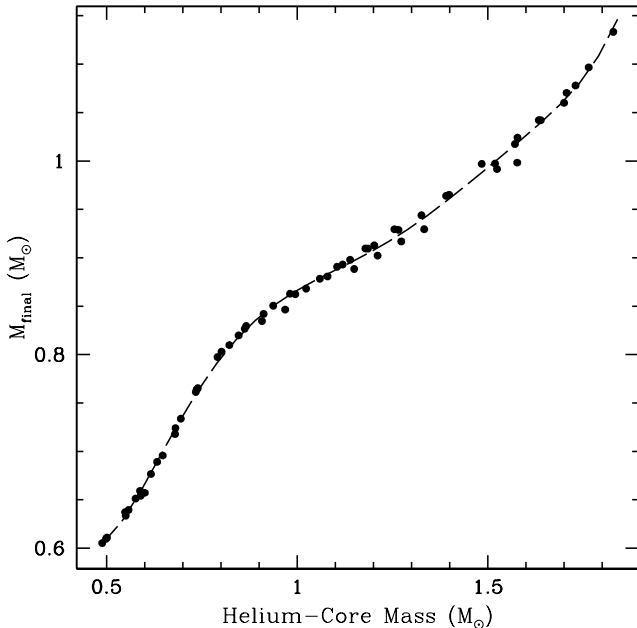


FIG. 4.— MIST model relation between helium-core mass at the beginning of the AGB and final WD mass. This relation is insensitive to rotation and has been applied to SYCLIST helium-core masses to further study the IFMR.

age rotation rates before the mixing becomes important. Therefore, this only systematically shifts the mean WD trend upward by  $0.02 M_{\odot}$  ( $M_{\text{initial}}$  of 3 to  $3.6 M_{\odot}$ ) and  $0.04 M_{\odot}$  ( $M_{\text{initial}}$  of  $3.6$  to  $6 M_{\odot}$ ). This alone is not enough to match observations.

The magnitude of rotational effects in models still remains poorly constrained. Therefore, we also consider the SYCLIST rotational models, which adopt more efficient rotational mixing. The SYCLIST models do not fully evolve to the WD cooling sequence, but at this intermediate-mass range, they all do evolve at least to the end of central helium burning (the beginning of the AGB). The phases before the AGB are where the direct effects of rotation are important. Stars have lost enough of their angular momentum before they reach the short AGB phase that any remaining variations in angular momentum no longer play a major role. However, more rapidly rotating stars at early stages do evolve more massive cores, and based on the MIST models the remaining core evolution during the AGB is predominantly sensitive to the helium-core mass, rather than the total mass, at the beginning of the AGB; differences in initial rotation and remaining envelope mass play no major role. Figure 4 illustrates the consistent relation between these two masses from MIST across all rotation rates.

We apply Figure 4’s relation to SYCLIST helium-core masses at the beginning of the AGB to quantify the SYCLIST IFMR’s sensitivity to rotation. In the middle-panel of Figure 3, the resulting IFMR for the non-rotating SYCLIST models are shown as green data points at  $M_{\text{initial}}$  of 2.5, 3, 4, and  $5 M_{\odot}$  and are comparable to that from MIST (dashed-blue). Applying the SYCLIST model’s rotational sensitivity to the consistent, but more complete, non-rotating MIST IFMR produces the synthetic IFMR distribution shown. Across this  $M_{\text{initial}}$  range the SYCLIST models give a more con-

sistent IFMR spread in  $M_{\text{final}}$ , and its density distribution is notably different with a weakly populated lower envelope and a densely populated upper envelope. This results from more efficient rotational mixing requiring little rotation to affect evolution, followed by rotational mixing reaching a saturation point at higher rotation, producing a concentration in the IFMR. The SYCLIST synthetic IFMR shifts the mean trend upward by  $\sim 0.06 M_{\odot}$ .

These two synthetic IFMRs still fall short of observations, but the ATON IFMR with increased CCO further increases core mixing. In the lower-panel of Figure 3, we apply the MIST rotational models to a smoothed ATON non-rotating IFMR. This produces a much stronger consistency with observations, with a mean trend shifted upward by  $\sim 0.08 M_{\odot}$  relative to the non-rotating MIST IFMR. However, unlike rotational-mixing, CCO does not increase scatter. Additionally, note that increased CCO also extends a star’s lifetime, but unlike rotation it uniformly affects all stars of a given mass and systematically affects derived cluster age, so it does not significantly affect the inference of  $M_{\text{initial}}$  (see Paper I).

### 3.2. Monte Carlo Analysis

Monte Carlo analysis provides a more powerful comparison between a synthetic IFMR and observations. For each synthetic IFMR model from Figure 3, we first apply an  $M_{\text{initial}}$  distribution based directly on the data (power law of exponent =  $-2.45$ ) and generate 10 million WDs. Second, we apply a distribution of observational errors based directly on the data. Third, to match the observed statistics, we match the observed numbers by drawing 29 intermediate-mass synthetic WDs ( $2.7 < M_{\text{initial}} < 3.6 M_{\odot}$ ) and 34 higher-mass synthetic WDs ( $3.6 < M_{\text{initial}} < 6.5 M_{\odot}$ ). By synthetically applying the observational errors, numbers, and  $M_{\text{initial}}$  distribution to each evolutionary and rotational model, we can more directly compare to the semi-empirical IFMR trends and scatter.

In Figure 5’s left panels, for each synthetic IFMR model, we illustrate on the x-axis each intermediate- and high-mass synthetic sample’s mean  $M_{\text{final}}$  offset from the non-rotating MIST IFMR. On the y-axis we illustrate the corresponding  $\sigma$  relative to each synthetic IFMR’s 2-piece fit in Figure 3. We illustrate each distribution’s central peak and 1, 2, and  $3\sigma$  contours, and this shows how these parameters are correlated. We represent the distributions for MIST models with no applied rotation in blue and full rotational models in green, SYCLIST rotational models in gold, and MIST rotational models applied to the smoothed non-rotating ATON IFMR in black. These are compared to the semi-empirical IFMR in purple. In the right panels, histograms of the resulting  $M_{\text{final}}$  scatter distribution shapes show MIST rotational models with their concentration on the lower envelope and SYCLIST rotational models with their concentration on the upper envelope.

This illustrates the impact of rotation in IFMR analysis and the resulting differences between models. Additionally, the MIST/ATON combination can recreate the high-mass observations within  $2\sigma$  and the intermediate-mass observations within  $3\sigma$ , but the synthetic scatter remains typically smaller. Additionally, the right panels show that the model distribution shapes are comparable to observations, but at higher masses the MIST/ATON



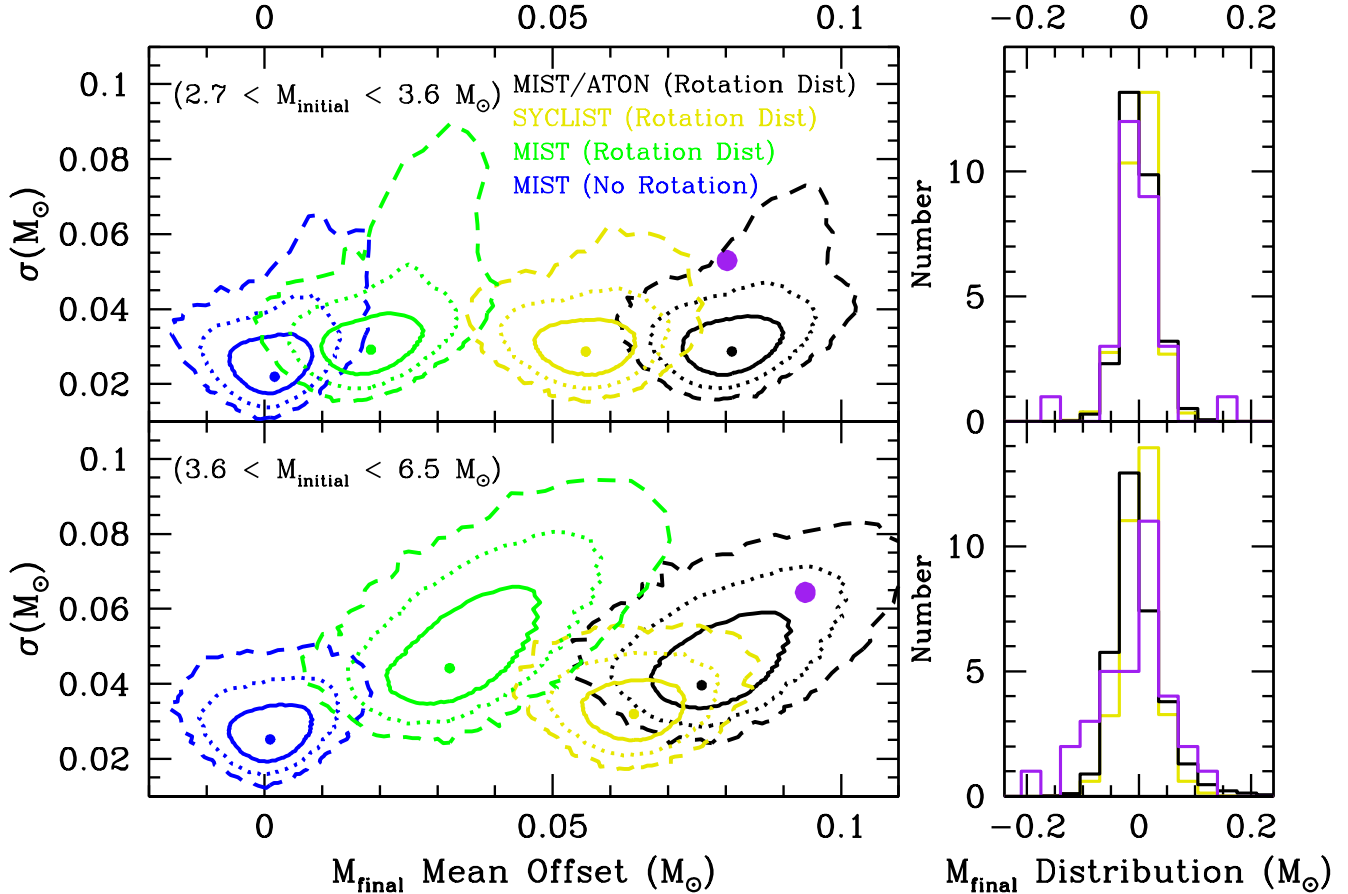


FIG. 5.— Observational errors and an IMF are applied to the synthetic IFMRs. Monte Carlo analysis of these distributions are performed by drawing the same number of synthetic WDs that have been observed at intermediate and high masses (upper and lower panels, respectively). 2D contours representing the distribution peaks and 1 (solid), 2 (dotted), and 3 (dashed)  $\sigma$  show that with MIST rotation applied to the ATON IFMR (black), it can match observations (purple), but that the observed scatter is only partially explained. The right panels illustrate the  $M_{\text{final}}$  residual distributions relative to observations (purple).

model’s distribution appears inconsistent.

#### 4. SUMMARY

The semi-empirical IFMR is a valuable constraint of stellar evolution. Comparisons to various recent models show that at the lowest masses ( $M_{\text{initial}} < 3 M_{\odot}$ ) there are still important differences in predicted  $M_{\text{final}}$ . At lower masses these differences predominantly result from how these models handle the AGB. Significant limitations remain in the low-mass data, however, currently making it challenging to constrain these models, but appropriate adjustments to AGB parameters alone will likely be able to explain low-mass observations. Additionally, at these lower masses, an intrinsic IFMR scatter is likely not needed because the intracluster scatters are consistent with observational errors (Paper I, Williams et al. 2018). Consistent with this, at lower masses the effects of rotation on core evolution are not strong enough to produce an intrinsic scatter.

For intermediate and higher masses (3 to  $6.5 M_{\odot}$ ), the theoretical IFMRs are less sensitive to the AGB model parameters. In comparison to observations, nearly all models predict WDs masses  $\sim 0.1 M_{\odot}$  below observations. Realistic changes in mass-loss rates and 3DUP efficiencies can play some role but likely cannot explain this difference nor the increased scatter. The ATON models, however, do show that efficient exponentially diffusive

CCO is a powerful way to help match, but not fully explain, observations.

All of these models, however, have assumed non-rotating progenitors. Therefore, we have demonstrated in this letter the effects that progenitor rotation will have on the IFMR. Applying the effects of rotation from either the MIST or SYCLIST rotational models to a non-rotating IFMR shows that through the broad range of B-dwarf rotations, both models predict a broad IFMR scatter but with important differences; the MIST models with less efficient rotational-mixing predict a higher concentration of stars on the distribution’s lower envelope while the SYCLIST models predict a higher concentration of stars on the upper envelope. These result in systematically higher WD masses relative to the non-rotating model, with MIST models shifting 0.02 to  $0.04 M_{\odot}$ , SYCLIST models shifting  $0.06 M_{\odot}$ , and MIST/ATON models shifting  $0.08 M_{\odot}$ .

Applying observational errors, an IMF, and the Monte Carlo method to these synthetic IFMRs shows that these rotational models can also explain most, but likely not all, of the observed scatter being larger than observational errors. Therefore, further refinement of rotational mixing efficiencies may be needed, but we note that the effects of environment, field contaminants, or merger remnants could also be the cause of this increased ob-

served IFMR scatter. More cluster white dwarf data are needed to study this further because other available methods to constrain the IFMR, e.g., with Gaia (El-Badry et al. 2018), are unable to characterize the IFMR scatter. This letter, however, illustrates that the semi-empirical IFMR is a powerful tool for constraining the effects of rotation and CCO on the core evolution of stars.

**Acknowledgments:** This project was supported by the National Science Foundation through grant AST-1614933 and the European Research Council under the European Union’s Horizon 2020 research and innovation programme n. 677706 (WD3D).

## REFERENCES

- Brandt, T. D., & Huang, C. X. 2015, *ApJ*, 807, 25
- Choi, J., Dotter, A., Conroy, C., et al. 2016, *ApJ*, 823, 102
- Choi, J., Conroy, C., & Byler, N. 2017, *ApJ*, 838, 159
- Cummings, J. D., Kalirai, J. S., Tremblay, P.-E., & Ramirez-Ruiz, E. 2016a, *ApJ*, 818, 84
- Cummings, J. D., Kalirai, J. S., Tremblay, P.-E., Ramirez-Ruiz, E., & Bergeron, P. 2016b, *ApJ*, 820, L18
- Cummings, J. D., Deliyannis, C. P., Maderak, R. M., & Steinhauer, A. 2017, *AJ*, 153, 128
- Cummings, J. D., & Kalirai, J. S. 2018, *AJ*, 156, 165
- Cummings, J. D., Kalirai, J. S., Tremblay, P.-E., Ramirez-Ruiz, E., & Choi, J. 2018, *ApJ*, 866, 21 (Paper I)
- D’Antona, F., Di Criscienzo, M., Decressin, T., et al. 2015, *MNRAS*, 453, 2637
- Doherty, C. L., Gil-Pons, P., Lau, H. H. B., Lattanzio, J. C., & Siess, L. 2014, *MNRAS*, 437, 195
- Dominguez, I., Straniero, O., Tornambe, A., & Isern, J. 1996, *ApJ*, 472, 783
- Dotter, A. 2016, *ApJS*, 222, 8
- El-Badry, K., Rix, H.-W., & Weisz, D. R. 2018, *ApJ*, 860, L17
- Georgy, C., Ekström, S., Granada, A., et al. 2013, *A&A*, 553, A24
- Georgy, C., Granada, A., Ekström, S., et al. 2014, *A&A*, 566, A21
- Hermes, J. J., Gänsicke, B. T., Kawaler, S. D., et al. 2017, *ApJS*, 232, 23
- Huang, W., Gies, D. R., & McSwain, M. V. 2010, *ApJ*, 722, 605
- Hunter, I., Brott, I., Langer, N., et al. 2009, *A&A*, 496, 841
- Kalirai, J. S., Hansen, B. M. S., Kelson, D. D., et al. 2008, *ApJ*, 676, 594
- Kalirai, J. S., Marigo, P., & Tremblay, P.-E. 2014, *ApJ*, 782, 17
- Karakas, A. I., & Lugaro, M. 2016, *ApJ*, 825, 26
- Kawaler, S. D. 2015, 19th European Workshop on White Dwarfs, 493, 65
- Kilic, M., Gianninas, A., Bell, K. J., et al. 2015, *ApJ*, 814, L31
- Koester, D., & Weidemann, V. 1980, *A&A*, 81, 145
- Koester, D., Dreizler, S., Weidemann, V., & Allard, N. F. 1998, *A&A*, 338, 612
- Langer, N. 2012, *ARA&A*, 50, 107
- Maeder, A., & Meynet, G. 2000, *ARA&A*, 38, 143
- Marigo, P., & Girardi, L. 2007, *A&A*, 469, 239
- Marigo, P., Bressan, A., Nanni, A., Girardi, L., & Pumo, M. L. 2013, *MNRAS*, 434, 488
- Neiner, C., Mathis, S., Saio, H., et al. 2012, *A&A*, 539, A90
- Niederhofer, F., Georgy, C., Bastian, N., & Ekström, S. 2015, *MNRAS*, 453, 2070
- Proffitt, C. R., Lennon, D. J., Langer, N., & Brott, I. 2016, *ApJ*, 824, 3
- Rosen, A. L., Krumholz, M. R., & Ramirez-Ruiz, E. 2012, *ApJ*, 748, 97
- Salaris, M., Serenelli, A., Weiss, A., & Miller Bertolami, M. 2009, *ApJ*, 692, 1013
- Talon, S., Zahn, J.-P., Maeder, A., & Meynet, G. 1997, *A&A*, 322, 209
- Ventura, P., Karakas, A., Dell’Agli, F., García-Hernández, D. A., & Guzman-Ramirez, L. 2018, *MNRAS*, 475, 2282
- Weidemann, V. 2000, *A&A*, 363, 647